ACI JOURNAL TECHNICAL PAPER

Title no. 83-48

Confined Compression Tests of Cement Paste and Concrete up to 300 ksi

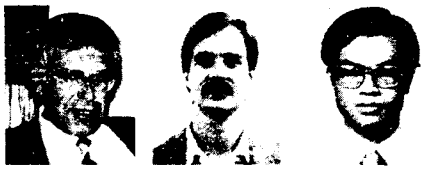

by Zdeněk P. Bažant, Finley C. Bishop, and Ta-Peng Chang

Tests of cylindrical specimens of 0.75 in. diameter up to 300,000 psi axial compression stress have been conducted for hardened portland cement paste as well as concrete with ⅜ in. aggregate. The specimens tightly fit into a cylindrical cavity in a pressure vessel and are loaded axially by a hard piston. The pressure vessel is very stiff, forcing the lateral expansion of specimens to be so small that the strain is almost uniaxial. Sophisticated analysis is used to evaluate material properties from measurements of force and displacement on the loading piston outside the test cavity. The results indicate that an initial decrease of the tangent modulus is followed by a continuous increase reaching values that exceed the initial modulus. This stiffening is attributed to pore closure; however, not all pores can yet be closed at the peak pressure. Unloading and reloading reveals relatively low hysteresis at these high pressures. Reloading beyond the previous maximum strain returns the response to the virgin diagram. Creep is found to exist at these high pressures, with a similar value of creep coefficient as that applicable for the service stress range. The results are presented in the form of diagrams as well as smoothing formulas. The tests reproduce well and the scatter is small.

Keywords: cement pastes; compression tests; concretes; creep properties; hysteresis; stress-strain diagram; tangent modulus.

Improved knowledge of the behavior of hardened portland cement paste and concrete at very high pressures is needed for two purposes: 1) to attain good understanding of the microstructure and mechanical properties of the material, and 2) to predict the behavior of certain special concrete structures subjected to very powerful explosions or projectile impact. Among the triaxial compression tests reported in the literature,[1-5] the highest compressive stresses were apparently reached by Chinn and Zimmerman.[6] In their tests, the principal stresses reached $\sigma_1 = -177{,}000$ psi, $\sigma_2 = \sigma_3 = -75{,}000$ psi (1 psi = 6895 Pa). In the tests of Balmer,[7] the maximum stresses were $\sigma_1 = -78{,}000$ psi, $\sigma_2 = \sigma_3 = -25{,}000$ psi, and in the tests of Green and Swanson,[8] $\sigma_1 = -15{,}120$ psi, $\sigma_2 = \sigma_3 = -2000$ psi. All these tests were standard triaxial tests in which the lateral normal stresses provided by fluid pressure are kept constant while the axial compression is increased. The stress-strain diagram in these tests exhibits a gradually declining slope, i.e., the incremental stiffness softens.

The standard triaxial test, however, does not closely simulate the conditions of concrete in structures designed to resist explosions on impact. In these structures, concrete is confined by heavy reinforcement in three directions, which causes the lateral normal stresses to increase along with the axial stress. The behavior of concrete in these structures is better simulated by confined compression tests. The simplest to evaluate, but hard to realize, would be the uniaxial strain test in which the lateral strains are forced to be zero. Typical practical situations are better simulated by an elastically confined test in which concrete is permitted to expand laterally while the lateral normal stresses increase. Such tests are also easier to carry out, particularly at very high pressures.

Various important questions arise with regard to high pressure behavior. Does the slope of the stress-strain diagram decrease or increase in an elastically confined test? Does any peak stress and post-peak softening exist? What equation describes the stress-strain diagram? Does concrete at very high pressures exhibit hysteresis, and what is its energy absorption capability? Does concrete creep and does it show a rate effect at such pressures?

To answer such questions, confined compression tests of small cylindrical specimens loaded axially up to 300,000 psi (i.e., 2068 MPa or 21,090 kip/cm^2) have been carried out and anlayzed at the Center for Concrete and Geomaterials of Northwestern University. In what follows, these tests are described and the results are reported.

Received Oct. 1, 1984, and reviewed under Institute publication policies.
Copyright © 1986, American Concrete Institute. All rights reserved, including the making of copies unless permission is obtained from the copyright proprietors. Pertinent discussion will be published in the May-June 1987 ACI JOURNAL if received by Feb. 1, 1987.

Zdeněk P. Bažant, FACI, is a professor and director, Center for Concrete and Geomaterials, Northwestern University. Dr. Bažant is a registered structural engineer, serves as consultant to Argonne National Laboratory and several other firms, and is on editorial boards of five journals. He is Chairman of ACI Committee 446, Fracture Mechanics, and a member of ACI Committee 209, Creep and Shrinkage in Concrete; 348, Structural Safety; and joint ACI-ASCE Committee 334, Concrete Shell Design and Construction. He also serves as Chairman of RILEM Committee TC69 on creep, of ASCE-EMD Committee on Properties of Materials, and of IA-SMiRT Division H. His works on concrete and geomaterials, inelastic behavior, fracture and stability have been recognized by a RILEM medal, ASCE Huber Prize and T. Y. Lin Award, IR-100 Award, Guggenheim Fellowship, Ford Foundation Fellowship, and election as Fellow of American Academy of Mechanics.

Finley C. Bishop is an associate professor of geological sciences at Northwestern University. He received his AB from Carleton College in 1972, his MS from the University of Chicago in 1974, and his PhD in geophysical sciences from the University of Chicago in 1976. He has been at Northwestern University since 1976. His current research focuses on the chemical and physical properties of minerals at high pressures and temperatures.

Ta-Peng Chang is a structural engineering specialist at Sargent and Lundy Engineers, Chicago, Ill. He obtained his BS from the National Taiwan Institute of Technology, MS from the University of Washington, Seattle, and a PhD from Northwestern University. He has been involved in harbor construction and in analysis of nuclear reactor containment structures. His research interests include constitutive models, strain-softening behavior, and finite element analysis.

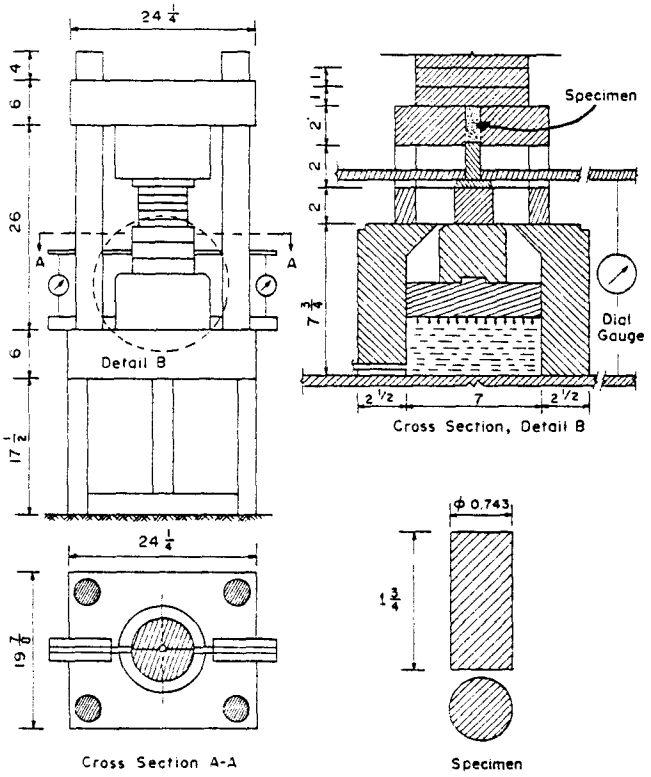

Fig. 1—Testing machine (developed by F. Bishop) and the test specimen (all length in inches)

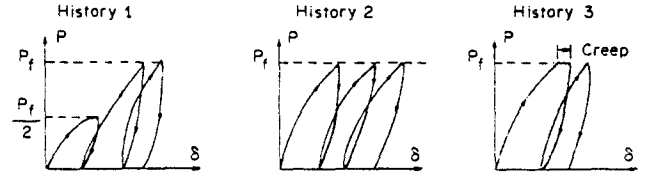

Fig. 2—Load histories used in tests

TESTING MACHINE

The project used a testing machine (Fig. 1) which was previously designed and built by F. Bishop in the Department of Geological Sciences for the original purpose of testing chemical reactions in molten rock at conditions prevailing in the earth mantle. The machine was modified to carry out the present tests at room temperature (73 F).

The material is tested in a pressure vessel with a cylindrical cavity of 0.75 in. in diameter and 2 in. long (1 in. = 25.4 mm). The cylindrical wall of the pressure vessel consists of three tightly fitted cylinders of 2 in. thickness each. The innermost cylinder is made of tungsten carbide steel that has an extremely high Young's modulus (105) $\times$ 10^6 psi). The middle and outer cylinders are hardened tool steel (No. 4340) rings. A soft steel safety ring surrounds the three cylinders. The cylindrical specimen, placed in the cavity, is loaded axially from below by a tip-tapered tungsten carbide piston of 0.75 in. diameter, provided at the piston's top with a sealing ring. Pressure is produced by a hydraulic ram and pressure intensifier. The piston is driven by a master ram at the bottom (Fig. 1). Underneath the pressure vessel, two steel rings of 8 in. external diameter and 1 in. thickness are piled up to provide vertical support for the pressure vessel. Since this machine had not originally been designed for any deformation measurements, lateral arms for measuring axial movement of the piston had to be attached. To make this possible, the upper supporting ring had to be sawed apart into two semicircular parts spread apart to provide openings for the displacement measuring arms stretching to the outside. One dial gage was attached to each arm to measure the vertical displacement of the piston. Detailed designs of the apparatus are available from the authors.

Due to its large mass and the use of tungsten carbide, the pressure vessel is extremely stiff and undergoes only small lateral expansion due to pressurizing the specimen. The lateral confining pressure is obtained as a reaction of the pressure vessel opposing the lateral expansion of the specimen. The lateral expansion is so small that the test conditions are quite close to uniaxial strain. The ratio of the maximum lateral strain to the maximum axial strain was observed to be about 0.005, which is about 40 times less than the elastic Poisson ratio.

TEST SPECIMENS AND LOADING PATHS

The tests included both hardened cement paste and concrete specimens. The specimens were solid cylinders of diameter 0.743 in. and 1.75 in. length. The water-cement ratio was w/c = 0.5, and the concrete mix had the ratio sand-aggregate-cement = 2:2:1 by weight. A portland cement of Type I meeting the ASTM C 150 specification was used. The maximum size of the aggregate was ⅜ in. and the maximum sand size was ⅛ in. Mineralogically, the aggregate was crushed limestone conforming to ASTM No. 7 designation. The specimens were cast in brass forms, vibrated, and then

placed in a sealed plastic container containing water at the bottom for the first 24 hr of curing. Afterwards, the specimens were taken out of the forms and placed in a fog room at 75 F where they were kept until testing.

The age of the specimens at the time of the test was 281 days, with deviations ± 8 days. The uniaxial compression strength of the cement paste specimens was 7150 psi, and of the concrete specimens was 5060 psi (mean values), when loaded through unlubricated steel platens. The Young's elastic moduli of the cement paste and concrete specimens were 2,079,000 and 5,325,000 psi, respectively.

Before insertion into the test cavity, the specimen was wrapped in a single layer of thin lead foil (of 0.0035 in. thickness). The lead foil flows plastically under the pressures in the cavity, thus reducing the friction against the walls. It also provides a smooth distribution of lateral pressure on the specimen surface. Furthermore, the layer of lead facilitates pushing the specimen out of the test cavity after the test. Before doing this the pressure vessel with the tested specimen must be removed from the machine.

LOAD HISTORIES AND RESPONSE MEASURED

Three types of load histories, shown in Fig. 2, were used. For each load history, three cement paste specimens and three concrete specimens were tested. History No. 1 includes unloading before the maximum stress is reached, and History No. 3 includes a two-hour period under the maximum load to observe creep.

In the present type of test, simplicity of test arrangement and measurement is traded for complexity of the theoretical evaluation of results. It would be much more difficult to measure the strain directly on the specimen inside the test cavity and the stress exactly at the end of the specimen. The axial strain of the specimen is deduced from the displacement measured by dial gages on the piston, and the stress in the specimen is calculated from the load on the piston. Thus, friction forces between the piston and the center of the specimen must be subtracted. The sum of these forces can be approximately determined from the rebound after the start of unloading and also from the force required to push the specimen out of the cylindrical cavity after the test, which was measured as well.

The axial strain on the specimen is obtained from the observed displacement of the piston δ_r, by subtracting the deformations contributed by the loading shaft, the expansion of the pressure vessel, and the combined deformation of the part of the loading system. These deformations were determined in advance by calibration tests in which an aluminum specimen of known properties was used. The calibration and theoretical evaluation of the results is described in detail in the Appendix.

After correcting the readings for the aforementioned extraneous influences, the response diagrams in Fig. 3 through 5 are obtained. Fig. 3 (a) through (f) show the responses for the individual specimens. Note that the responses for the specimens of each group subjected to the same loading history are very close to each other, which indicates good reproducibility and consistency of results. Fig. 3 (g) through (i) show the average strains for each group of three specimens.

DISCUSSION OF TEST RESULTS

From the response diagram in Fig. 3 through 5, the following observations can be drawn.

1. After an initial decrease, the slope of the loading diagram (Fig. 3) continuously increases, i.e., after an initial softening, the response stiffens. This stiffening continues all the way to 300,000 psi and a constant slope is apparently not yet reached. The initial softening (decrease of slope) is no doubt caused by breakage of pore walls and collapse of the pores, while the subsequent stiffening is due to closure of pores, probably just the capillary pores. The minimum slope is achieved, for both concrete and hardened cement paste, at roughly 50,000 psi axial compression. This means that the rate of pore collapse is at this point approximately equal to the rate of pore closures.

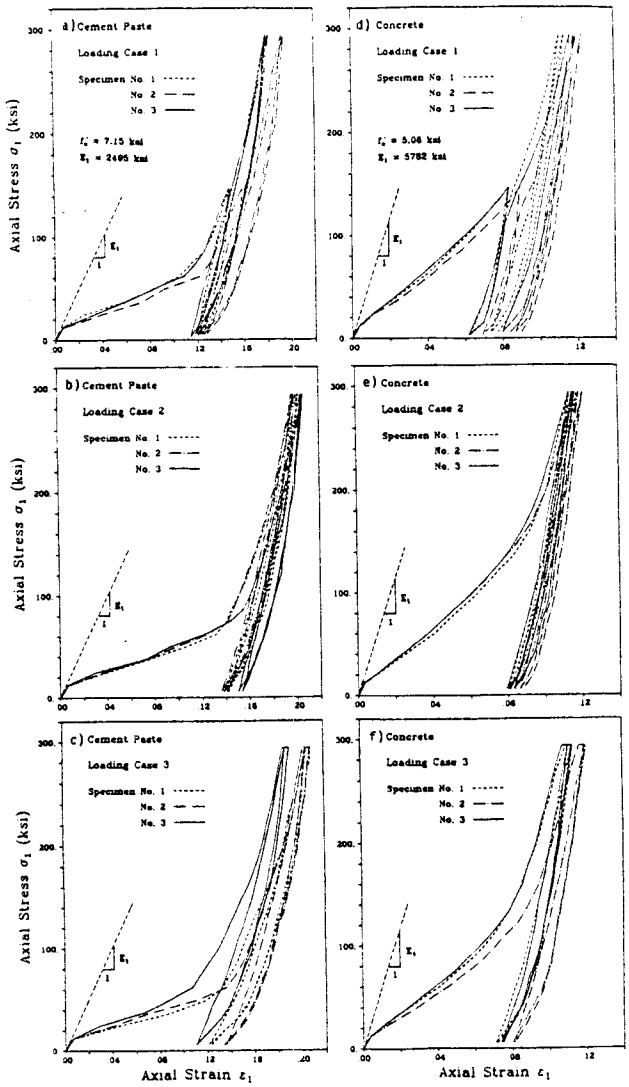

Fig. 3(a)-(f)—Stress-strain diagrams determined from measurements

2. Based on the measured axial strain and a small lateral strain deduced from the expansion of the pressure vessel, the total relative decrease of volume at 300,000 psi is about 20 percent. The volume fraction of capillary pores in a hardened portland cement paste of water-cement ratio was estimated as 26 percent.[9] This means that at 300,000 psi, the volume fraction of (capillary) pores still represents about 6 percent of the material volume, which amounts to about 23 percent of the original volume of the capillary pore space.

3. The initial slopes E_1 marked in Fig. 3 represent the theoretical elastic modulus for uniaxial strain, which is calculated as $E_1 = E_0(1 - \nu)/[(1 + \nu)(1 - 2\nu)]$ in which ν = elastic Poisson ratio (roughly 0.18 for concrete and 0.25 for hardened cement paste). The final slopes of the diagrams in Fig. 3 are steeper than E_1; for concrete they are about 1.5 times higher, and for cement paste about 2 times higher. Thus, the cement paste undergoes relatively more stiffening at very high pressures than does concrete. However, the cement paste also undergoes more softening (a greater relative decrease of slope) at intermediate pressure around 50,000 psi [Fig. 3(a),(b), and (c)].

4. The slope of the final tangent of the loading diagram (at 300,000 psi) is approximately equal to the mean unloading slope for both concrete and cement paste. The initial slope of the unloading diagram is about 1.6 times higher than the final slope of the loading diagram in the case of concrete, and 1.8 times higher in the case of cement paste [Fig. 3(g),(h), and (i)].

5. The path of reloading after previous unloading returns approximately to the virgin loading path after the strain at the previous maximum stress is exceeded [Fig. 3(a),(d), and (g)]. This behavior is the same as that known for the low pressure range.

6. There is hysteresis, with the associated loss of energy, even at these high pressures. The energy loss (the area enclosed by the loop of the stress-strain diagram) is relatively small. During the first cycle the loss is about $0.05W_1$ for both concrete and cement paste, W_1 being the work done on the material up to the maximum stress (300,000 psi), equal to the area under the rising stress-strain diagram [Fig. 3(g) and (h)].

7. Even at these high pressures, hardened cement paste as well as concrete does exhibit creep [Fig. 3(i)]. The creep coefficient (i.e., the ratio of the strain increment to the initial strain) is for a two-hour loading period about 0.25 of that for the linear, service stress range (i.e., about 2000 psi in uniaxial compression). Although the shape of the creep curve in Fig. 4 may have been influenced by changes of friction, it seems that a logarithmic law would describe the creep curve better than a power law; however, for a small exponent of the power law, such as 0.05, the difference is very small. The creep curves in Fig. 4 may be approximately described by the formula

$$\epsilon_1 = \sigma_1[a + b \log \bar{t}] \qquad (1)$$

in which $\bar{t}$ = load duration in minutes, $a = 3.77 \times 10^{-7}$/psi; $b = 8.13 \times 10^{-9}$/psi for concrete, and $a = 6.63 \times 10^{-7}$/psi; $b = 13.1 \times 10^{-9}$/psi for cement paste.

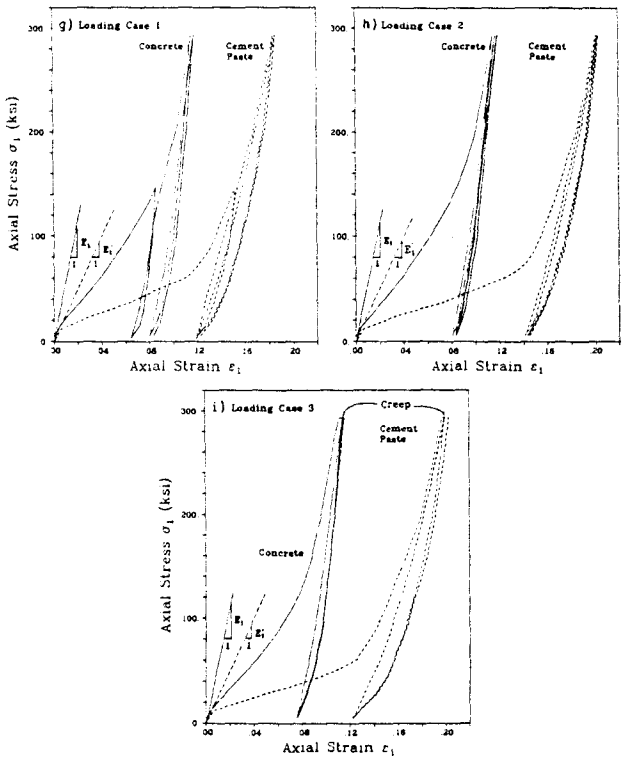

Fig. 3(g)-(i)—Average stress strain diagrams determined from measurements

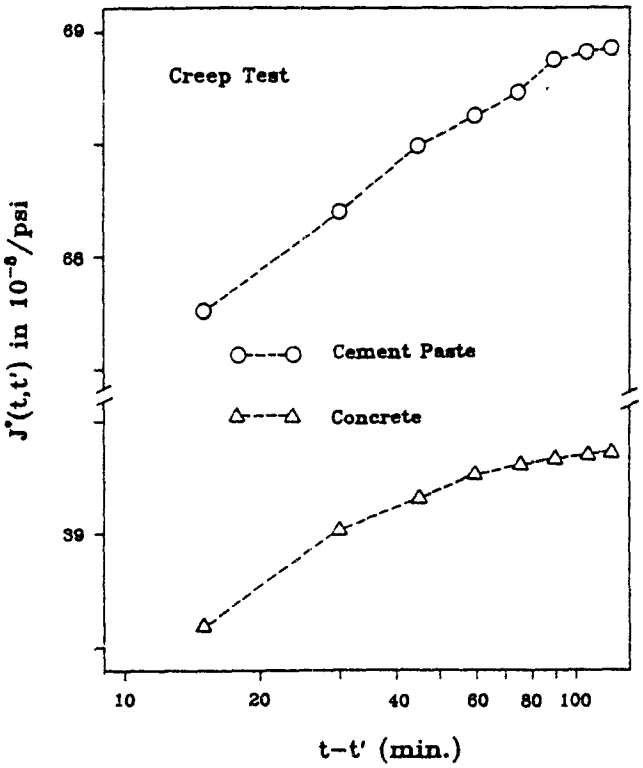

Fig. 4—Creep at maximum stress plotted as compliance function for elastic confinement

The creep strains observed have been assumed to be approximately the same as for a constant load that is applied suddenly. The creep formula in Eq. (1) may also serve as an indication of the rate effect and may probably be extrapolated to shorter times using a plot in the logarithmic time scale. [The logarithmic law is well known for rocks at low temperatures and is in geology called the Lomnitz creep law (see Reference 4 or 11)].

8. Reloading to the same peak stress leaves some permanent deformation even at these high pressures. However, this permanent deformation appears to be due to creep rather than plasticity because it is approximately equal to the creep deformation during the time it took to unload and reload the specimen.

The response curves obtained from the present tests may be approximately described by the following empirical formulas:

Virgin loading

$$\sigma_1 = a_1\epsilon_1 + a_2\epsilon_1^2 + a_3\epsilon_1^3 + a_4\epsilon_1^4 \quad (2)$$

First unloading

$$\sigma_1 = \sigma_b - \frac{\epsilon - \epsilon_b}{\epsilon_f - \epsilon_b}[\sigma_b + a_5(\epsilon_f^2 - \epsilon_b^2) - \sigma_f] + a_5(\epsilon^2 - \epsilon_b^2) \quad (3)$$

$$\sigma_1 = \sigma_f - \frac{\epsilon - \epsilon_f}{\epsilon_b - \epsilon_f}[\sigma_f + a_6(\epsilon_b^2 - \epsilon_f^2) - \sigma_b] + a_6(\epsilon^2 - \epsilon_f^2) \quad (4)$$

in which σ_1 = axial stress, ϵ_1 = axial strain; ϵ_b, σ_b, ϵ_f, σ_f = axial strain and stress values at the beginning of unloading and at the beginning of reloading; and a_1, a_2, . . . a_6 = empirical constants found by fitting the mean data in Fig. 5. The values of these constants for cement paste are 1001, −5935, −33,290, 370,800, 81,480, 27,090 psi, and for concrete, 1578, 13,760, −427,100, 3,346,000, 143,900, and 56,740 psi, respectively. For these values the preceeding formulas are plotted in Fig. 5 and are compared with the measured mean data points.

It must be emphasized that the foregoing empirical formulas apply to the present type of elastic confinement and not, for example, to hydrostatic compression. The purpose of these formulas is to provide a smooth response diagram that can be used in fitting a constitutive law.

Due to the damage to the specimen caused by pushing it out of the pressure vessel after the test in a separate hydraulic press, strength measurements after the test are difficult to interpret. Nevertheless, it appears that the strength is not increased in the present type of elastically confined compression test. It is true that hydrostatic pressure generally increases the strength; however, deviatoric (shear) deformation decreases the strength, and in the present type of test both occur simultaneously.

CONCLUSION

The elastically confined compression test is a feasible means of determining the deformations of concrete and cement paste at extremely high pressures. The measurements are reproducible and exhibit little scatter; however, a sophisticated theoretical analysis is required to determine material properties from the measurements.

ACKNOWLEDGMENTS

The experimental work was supported under National Science Foundation grant EAR-8108589 (FCB) (F. Bishop, Principal Investigator and Director). The specimen preparation, some machine modifications, the conduct of tests, and the theoretical analysis were supported under National Science Foundation Grant No. CEE800-3148 (Z. P. Bažant, Principal Investigator and Director).

REFERENCES

1. Cedolin, Luigi; Crutzen, Yves R. J.; and Dei Poli, Sandro, "Triaxial Stress-Strain Relationship for Concrete," *Proceedings*, ASCE, V. 103, EM3, June 1977, pp. 423-439.

2. Gerstle, Kurt H., et al., "Behavior of Concrete under Multiaxial Stress States," *Proceedings*, ASCE, V. 106, EM6, Dec. 1980, pp. 1383-1403.

3. Kotsovos, Michael D., and Newman, John B., "Generalized Stress-Strain Relations for Concrete," *Proceedings*, ASCE, V. 104, EM4, Aug. 1978, pp. 845-856.

4. Palaniswamy, R., and Shah, S. P., "Deformations and Failure of Hardened Cement Paste Subjected to Multiaxial Stresses," *Proceedings*, RILEM Symposium on Multiaxial Stresses, Cannes, Oct. 1972.

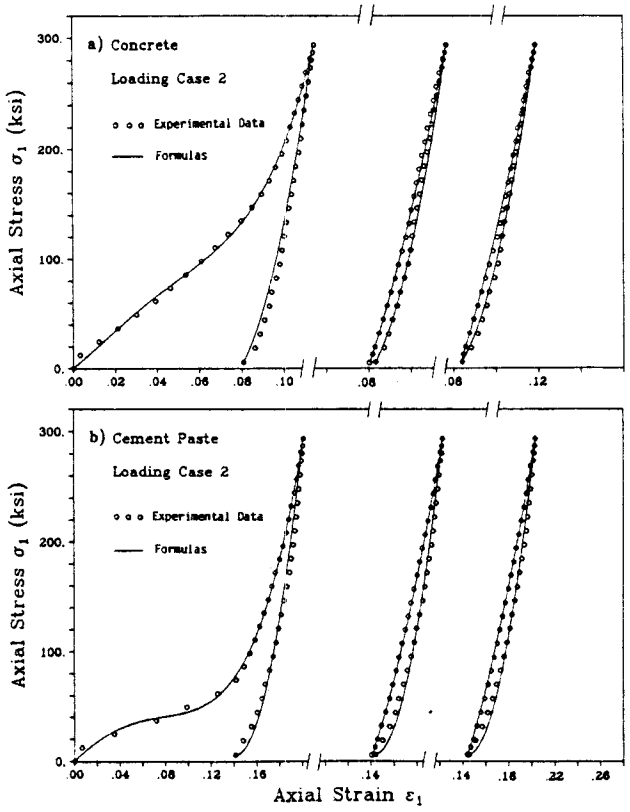

Fig. 5—Average response (data points) and its representation by formulas

5. Palaniswamy, Ranga, and Shah, Surendra P., "Fracture and Stress-Strain Relationship of Concrete under Triaxial Compression," *Proceedings*, ASCE, V. 100, ST5, May 1974, pp. 901-916.

6. Chinn, J., and Zimmermann, R. M., "Behavior of Plain Concrete under Various High Triaxial Compression Loading Conditions," *Technical Report* No. WL-TR64-163, Air Force Weapons Laboratory, Kirtland Air Force Base, Albuquerque, 1965.

7. Balmer, G. G., "Shearing Strength of Concrete under Triaxial Stress Computation of Mohr's Envelope as a Curve," *Report* No. SP-23, Structural Research Laboratory, U.S. Bureau of Reclamation, Denver, Oct. 1949.

8. Green, S. J., et al., "Static Constitutive Relations for Concrete," *Technical Report* No. AFWL-TR-72-244, Air Force Weapons Laboratory, Kirtland Air Force Base, Albuquerque, 1973.

9. Powers, T. C., "Structure and Physical Properties of Hardened Portland Cement Paste," *Journal*, American Ceramic Society, V. 41, No. 1, 1958, pp. 1-6. Also, *Research Department Bulletin* No. 94, Portland Cement Association.

10. Bolz, Ray E., and Tuve, George L., *Handbook of Tables for Applied Engineering Science*, Chemical Rubber Co., Cleveland, 1973, 974 pp.

11. Lomnitz, C., "Creep Measurements in Igneous Rocks," *Journal of Geology*, V. 64, 1956, pp. 473-478.

12. Roark, Raymond J., and Young, Warren C., *Formulas for Stress and Strain*, 5th Edition, McGraw-Hill Book Co., New York, 1975, 624 pp.

13. Weertman, J., and Weertman, J. R., "High Temperature Creep of Rock and Mantle Viscosity," *Annual Reviews of Earth and Planetary Science*, V. 3, 1975, pp. 283-315.

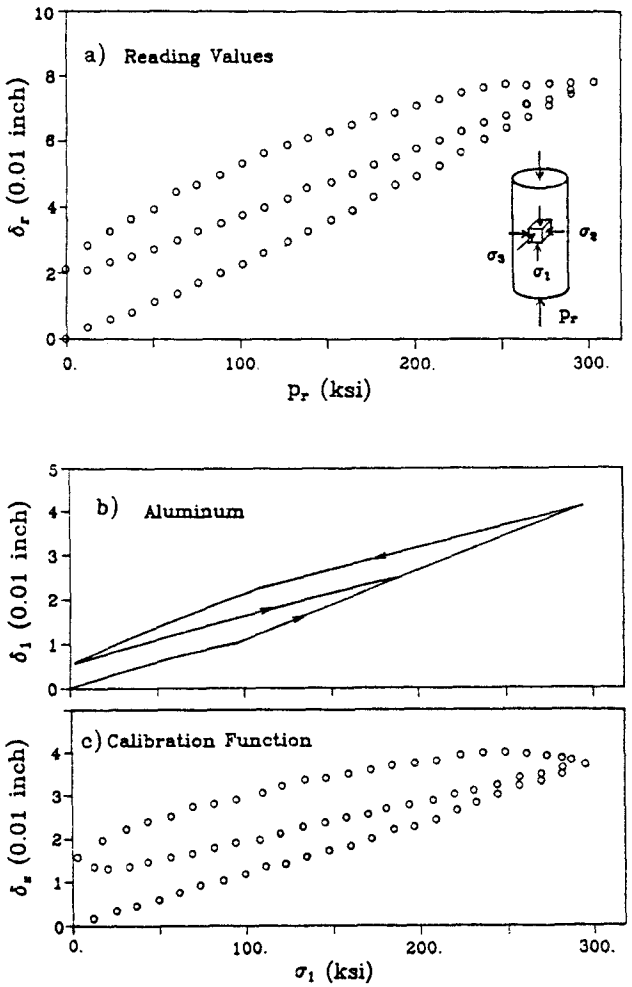

Fig. 6—Diagrams used in calibration of the tests by means of aluminum specimen

APPENDIX — Evaluation of material properties from measurements

Although the stress and strain in the specimen is not homogeneous, due to unavoidable friction on the specimen's surface, we assume it to be approximately homogeneous and equal to the stress and strain values at specimen midlength. These values, which are denoted as σ_1, ϵ_1 for the axial direction, and σ_2, ϵ_2 and σ_3, ϵ_3 for the lateral directions in cartesian coordinates x_1, x_2, x_3 may be expressed as

$$\sigma_1(P_r) = \frac{1}{A}[P_r - F(P_r)] \tag{5}$$

$$\epsilon_1(P_r) = \frac{1}{L}[\delta_r(P_r) - \delta_s(P_r)] \tag{6}$$

in which L = specimen's length, P_r = total force on the piston as read on the oil pressure gage, F = total axial friction force accumulated on the shaft and specimen surfaces between the piston and the specimen midlength, δ_r = displacement of the shaft at gage attachment points as read, δ_s = calibration function of the system = relative displacement accumulated in the loading shaft and the machine system between the gage attachment points and the specimen's ends, and A = cross section area of the specimen.

The calibration function $\delta_s(P_r)$ was determined by testing a specimen made of aluminum, the properties of which are known quite accurately. Aluminum at high pressures may be approximately described as an elastic-perfectly plastic material obeying von Mises yield criterion. Thus, the incremental constitutive relation for aluminum may be introduced as

$$d\epsilon_{ij} = \frac{d\sigma_0}{3K}\delta_{ij} + \frac{ds_{ij}}{2G} + d\lambda\frac{\partial f}{\partial \sigma_{ij}} \tag{7}$$

in which ϵ_{ij}, σ_{ij} = strain and stress tensors in cartesian coordinates x_i (i = 1, 2, 3), δ_{ij} = Kronecker delta, $\sigma_0 = \frac{1}{3}\sigma_{kk}$ = volumetric stress, $s_{ij} = \sigma_{ij} - \sigma_0\delta_{ij}$ = deviatoric stress tensor; K, G = elastic bulk and shear moduli of aluminum; and $f = (\frac{1}{2}s_{ij}s_{ij})^{\frac{1}{2}} - \tau_p$ = von Mises yield function (τ_p = shear yield stress = constant). Repeated subscripts imply summation over 1,2,3. The scalar multiplier $d\lambda$ can be determined from Prager's consistency condition $df = (\partial f/\partial\sigma_{ij})\,d\sigma_{ij} = 0$. By substituting into it Eq. (7) we get $d\lambda = (s_{mn}\,de_{mn})/\tau_p$, in which $e_{mn} = \epsilon_{mn} - \frac{1}{3}\epsilon_{kk}\delta_{mn}$ = deviatoric strain tensor. Thus, the incremental stress-strain relation is found to be

$$d\epsilon_{ij} = \frac{d\sigma_0}{3K}\delta_{ij} + \frac{ds_{ij}}{2G} + \frac{s_{mn}de_{mn}}{\tau_p^2}s_{ij} \tag{8}$$

or

$$d\sigma_{ij} = 2Gd\epsilon_{ij} + (3K - 2G)d\epsilon_0\delta_{ij} - G\frac{s_{mn}de_{mn}}{\tau_p^2}s_{ij} \tag{9}$$

Due to axial symmetry [Fig. 6(a)], we further have $\epsilon_2 = \epsilon_3$ and $\sigma_2 = \sigma_3$, and $\sigma_{12} = \sigma_{23} = \sigma_{31} = \epsilon_{12} = \epsilon_{23} = \epsilon_{31} = 0$. Accordingly, the stress-strain relation simplifies as follows

a. elastic range, $f < 0$

$$\begin{Bmatrix} d\sigma_1 \\ d\sigma_3 \end{Bmatrix} = \begin{bmatrix} D_{11} & D_{13} \\ D_{31} & D_{33} \end{bmatrix} \begin{Bmatrix} d\epsilon_1 \\ 2d\epsilon_3 \end{Bmatrix} \tag{10}$$

b. plastic range, $f = 0$

$$\begin{Bmatrix} d\sigma_1 \\ d\sigma_3 \end{Bmatrix} = \begin{bmatrix} C_{11} & C_{13} \\ C_{31} & C_{33} \end{bmatrix} \begin{Bmatrix} d\epsilon_1 \\ 2d\epsilon_3 \end{Bmatrix} \tag{11}$$

in which $D_{11} = K + \frac{4}{3}G$; $D_{13} = D_{31} = K - \frac{2}{3}G$; $D_{33} = K + \frac{1}{3}G$;

and

$$C_{11} = K + \frac{4}{3}G - \frac{4G}{9\tau_p^2}(\sigma_1 - \sigma_3)^2$$

$$C_{13} = C_{31} = D_{13} + \frac{2G}{9\tau_p^2}(\sigma_1 - \sigma_3)^2$$

$$C_{33} = D_{33} - \frac{G}{9\tau_p^2}(\sigma_1 - \sigma_3)^2 \quad (12)$$

Although the lateral expansion of the pressure vessel is quite small, it should be taken into account. The pressure vessel is designed to remain elastic, and so the lateral strain may be calculated as

$$\epsilon_3 = \frac{2u_r}{d_0} = \frac{\sigma_3}{B} \quad (13)$$

in which u_r is the radial displacement at the surface of the specimen, d_0 is the diameter of the specimen, and B is a constant, representing the elastic stiffness of the pressure vessel. The pressure vessel may be approximately considered to be in-plane strain, and then according to a well-known elasticity solution[12]

$$B = \frac{E_r}{1 + \nu_r}\frac{a^2 - b^2}{[b^2(1-2\nu_r) + a^2]} \quad (14)$$

in which E_r = Young's elastic modulus of tungsten carbide steel (= 105 x 10^6 psi), ν_r = Poisson ratio = 0.28, a = outer radius of pressure vessel = 4 in., b = inner radius of pressure vessel = 0.375 in. The contribution to B due to the two secondary confining steel rings outside the tungsten carbide ring has been neglected, and so the actual stiffness B was somewhat higher than Eq. (14) indicated.

Now, substitution of Eq. (13) into Eq. (10) and (13) gives

$$d\sigma_1 = E' d\epsilon_1 \quad (15)$$

with

$$E' = \frac{D_{11}(D_{33} - 0.5B) - D_{13}^2}{D_{33} - 0.5B} \quad \text{for elastic range} \quad (16)$$

$$E' = \frac{C_{11}(C_{33} - 0.5B) - C_{13}^2}{C_{33} - 0.5B} \quad \text{for plastic range} \quad (17)$$

Note that if the stiffness of the pressure vessel were infinite ($B \to \infty$), Eq. (15) would be for the elastic range

$$d\sigma_1 = E_1 d\epsilon_1 = (K + \frac{4}{3}G)\, d\epsilon_1 = \frac{E(1 - \nu)d\epsilon_1}{(1 + \nu)(1 - 2\nu)} \quad (18)$$

and for the plastic range

$$d\sigma_1 = C_{11}\, d\epsilon_1 \quad (19)$$

in which E = Young's elastic modulus and ν = Poisson ratio of the specimen. Eq. (18) is the same as for a uniaxial strain state.

Eq. (19) means that after the start of yielding the axial load is resisted in the aluminum specimen solely by elastic volume change, and shear yielding has no effect. Since the actual specimen condition is relatively close to the uniaxial strain state, we may conclude that shear

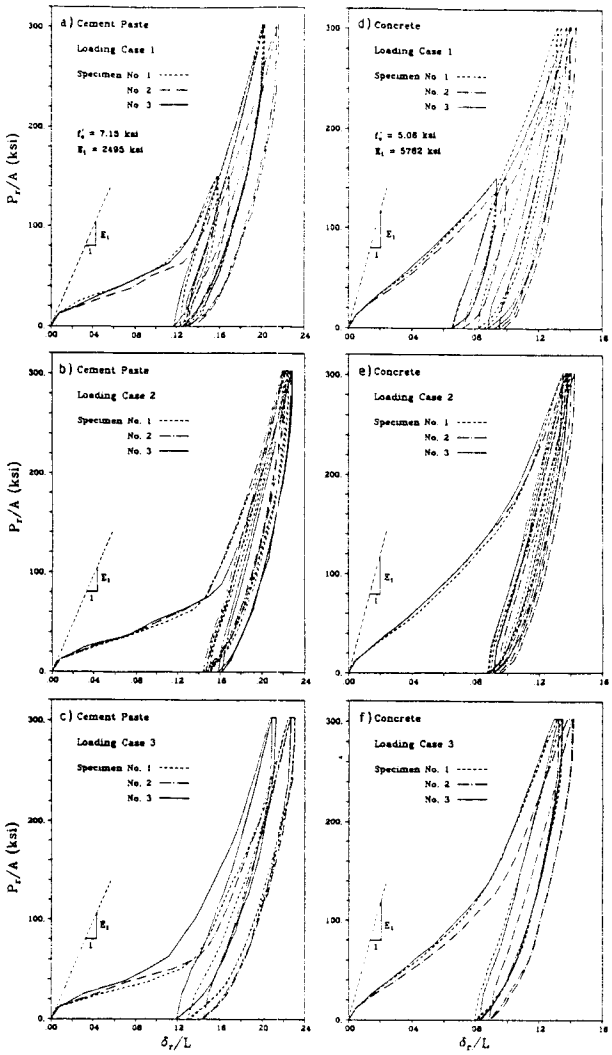

Fig. 7(a)-(f)—Originally measured data (without corrections for friction and deformation of system)

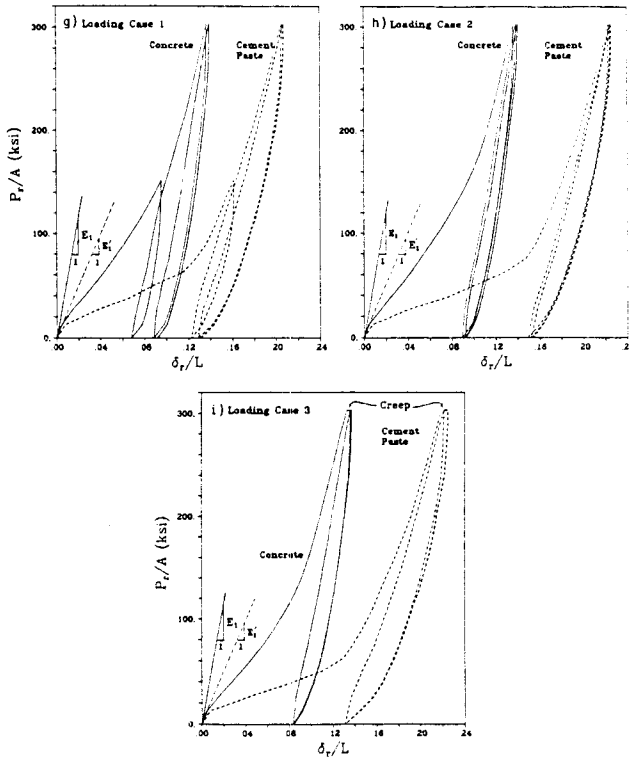

Fig. 7(g)-(i)—Average originally measured data (without corrections for friction and deformation of system)

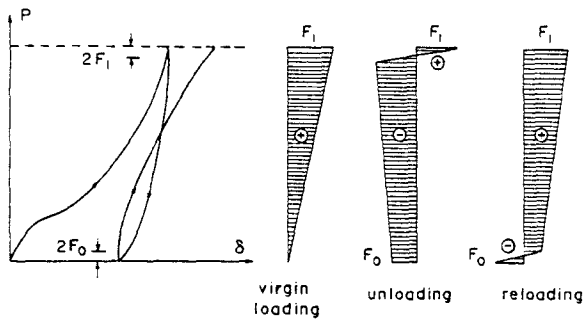

Fig. 8—Assumed variation of axial friction force

yielding of the aluminum specimen represents a relatively minor correction (for this reason the yield hardening of aluminum has been neglected).

The elastic volume change of aluminum is important for the calibration, and therefore nonlinearity of the compression diagram of aluminum has been taken into account [it is described by the relation $K = (10{,}390 + 70{,}500\ \epsilon_0)\ 10^6$ psi].[7] The other constants are $\tau_p = 47{,}000$ psi (shear yield stress of aluminum), $\tau = 0.34$, $L = 1.75$ in., and $A = 0.442$ in.^{2} According to Eq. (5) - (6), $d\sigma_i = (dP - dF)/A$, $d\epsilon_i = (d\delta_r - d\delta_i)/L$, and substituting this into Eq. (17) we obtain

$$d\delta_i(P_r) = d\delta_i(P_r) - \frac{L}{AE'(\sigma_i)}\left[dP_r - dF(P_r)\right] \qquad (20)$$

This equation defines in an incremental way the desired calibration function, $\delta_i(P_r)$. However, the friction force F must still be determined.

So as to simulate exactly the boundary conditions for the cement paste and concrete specimens, the aluminum specimen is also wrapped in the same lead foil. Thus, its surface friction may be considered to be about the same. The friction force may be estimated directly from the response diagram of the cement paste or concrete specimens. Its maximal value at peak stress equals about one-half of the drop in the force needed to start a retraction of the piston [the vertical segment at the beginning of unloading in Fig. (7)]. At the beginning of reloading, the friction force is obviously the same as the force needed to push the specimen out of the cylindrical vessel. This force was directly measured. At the start of first loading, the friction force may be assumed as zero. Between the extreme points, the friction force F may be supposed to vary linearly as a function of the load on the piston P_r. This yields the variation of the friction force as sketched in Fig. 8, and this variation is used in Eq. (20) as well as in determining the stress in the test specimens.

The maximum friction force at peak stress F_0 was found to be 4200 lb, and the friction force at the start of the loading (taken as one-half of the pushout force) was measured as 1235 lb. The latter value is less than that needed to cause yielding of the lead foil, probably because graphite lubricating powder was applied at the surface of the cavity. The shear yield stress of lead[8] is about 1900 psi, from which the total force needed to cause the lead foil to yield is $F_s = 1.9(0.75\pi)(1.75)/\sqrt{3} = 4.520$ lb and the total yield force up to the midlength of the specimen is $F_s/2 = 2260$ lb. Without the lead foil, the friction force values would no doubt be much more uncertain.

A computer program was written for step-by-step integration of the calibration function defined by Eq. (21). The result shown in Fig. 6(c) was then used in evaluating all the test results.

Finally, Fig. 7 presents the original test data consisting of the force P_r on the piston as read (divided by specimen cross section area A) and of displacement δ_r at the gage points of the loading shaft, as read (divided by specimen length L).